

Fourier-domain Green's function for an elastic semi-infinite solid under gravity, with applications to earthquake and volcano deformation

Sylvain Barbot* and Yuri Fialko

Institute of Geophysics and Planetary Physics, Scripps Institution of Oceanography, University of California San Diego, La Jolla, CA 92093-0225, USA.

E-mail: sbarbot@ucsd.edu

Accepted 2010 May 10. Received 2010 May 10; in original form 2009 October 6

SUMMARY

We present an analytic solution in the Fourier domain for an elastic deformation in a semi-infinite solid due to an arbitrary surface traction. We generalize the so-called Boussinesq's and Cerruti's problems to include a restoring buoyancy boundary condition at the surface. Buoyancy due to a large density contrast at the Earth's surface is an approximation to the full effect of gravity that neglects the perturbation of the gravitational potential and the change in density in the interior. Using the perturbation method, and assuming that the effect of gravity is small compared to the elastic deformation, we derive an approximation in the space domain to the Boussinesq's problem that accounts for a buoyancy boundary condition at the surface. The Fourier- and space-domain solutions are shown to be in good agreement. Numerous problems of elastostatic or quasi-static time-dependent deformation relevant to faulting in the Earth's interior (including inelastic deformation) can be modelled using equivalent body forces and surface tractions. Solving the governing equations with the elastic Green's function in the space domain can be impractical as the body force can be distributed over a large volume. We present a computationally efficient method to evaluate the elastic deformation in a 3-D half space due to the presence of an arbitrary distribution of internal forces and tractions at the surface of the half space. We first evaluate the elastic deformation in a periodic Cartesian volume in the Fourier domain, then use the analytic solutions to the generalized Boussinesq's and Cerruti's problems to satisfy the prescribed mixed boundary condition at the surface. We show some applications for magmatic intrusions and faulting. This approach can be used to solve elastostatic problems involving spatially heterogeneous elastic properties (by employing a homogenization method) and time-dependent problems such as non-linear viscoelastic relaxation, poroelastic rebound and non-steady fault creep under the assumption of spatially homogeneous elastic properties.

Key words: Numerical solutions; Mechanics, theory and modelling.

1 INTRODUCTION

An instantaneous deformation field accompanying an earthquake can be well explained assuming linear elastic deformation of the ambient rocks (Reid 1910; Fialko *et al.* 2001b; Simons *et al.* 2002; Fialko 2004). Post-seismic and inter-seismic phases of the earthquake cycle are also commonly modelled using solutions for an elastic half space (Savage 1974; McGuire & Segall 2003; Miyazaki *et al.* 2003; Hsu *et al.* 2006; Fialko 2006; Barbot *et al.* 2008b; 2009a). Elastic solutions are also widely used to model volcanic

unrest (e.g. Mogi 1958; Yang *et al.* 1988; Fialko *et al.* 2001a). Some types of time-dependent inelastic deformation can be simulated using an elastostatic Green's function by virtue of the Laplace transform whereby the time-series of deformation are obtained from a series of static deformation fields evaluated given the effective elastic moduli (Rundle 1982; Pollitz 1997; Wang *et al.* 2003, 2006; Smith & Sandwell 2004). Recent geodetic observations suggest that the time-dependent response of the crust and upper mantle to a stress perturbation may be in fact non-linear (Pollitz *et al.* 2001; Freed & Bürgmann 2004; Barbot *et al.* 2009a; Pearse & Fialko 2010). If so, models used to interpret observations of post-seismic deformation need to account for non-linear rheologies of the lower crust or upper mantle.

Barbot & Fialko (2010, submitted), hereafter referred to as the companion paper B&F, proposed a method to evaluate mechanisms

*Now at: Division of Geological and Planetary Sciences, California Institute of Technology, CA, USA.

thought to be involved in post-seismic transients (e.g. afterslip, viscoelasticity and poroelasticity), based on a fundamental solution for a body force in an elastic half space. In this paper, we present such a solution in the Fourier domain, to allow an efficient evaluation of the time-dependent displacement field by taking advantage of the fast Fourier transforms and the convolution theorem. The proposed semi-analytic method involves two steps: first we evaluate a displacement field in a full space, then apply a correction to satisfy the boundary condition (also, see Nguyen *et al.* 2008). Our model includes a mixed boundary condition with a gravitational restoring force that results from displacements across the density contrast interface. For typical wavelengths of coseismic deformation of the order of 10–100 km, the effect of gravity on surface displacements is several orders of magnitude smaller than the direct effect of rupture. For larger-wavelength post-seismic relaxation, the effect of gravity can be more prominent and the interior buoyancy forces are at least one order of magnitude smaller than the surface traction. Hereafter, we neglect the interior buoyancy restoring force associated with bulk compaction and extension. The method can be used to model post-seismic deformation involving non-linear rheologies (see companion paper B&F).

This paper is organized as follows. First, we describe a Fourier-domain analytic solution to the displacement field in a homogeneous elastic half-space under a prescribed traction boundary condition. The solution is obtained using the Galerkin vector potential. We consider the cases for tangential traction and normal load separately then describe a solution that accounts for an arbitrary spatial distribution of traction in all directions. Our solution generalizes the so-called Cerruti's and Boussinesq's problems to incorporate the buoyancy effect due to a density contrast at the surface. In Section 3, we derive a semi-analytic Green's function for the elastic half-space in the Fourier domain. Our formulation allows one to evaluate the displacement field due to an arbitrary distribution of internal forces and surface traction accounting for a buoyancy effect at the surface. In Section 4, we present applications relevant to crustal deformation and compare calculations using our method to known analytic solutions. We show an application of the proposed Green's function to deformation in a heterogeneous crust. In Appendix A, we use a perturbation method to derive an approximation to the solution to the generalized Boussinesq's problem in the space domain. We use this analytic solution to validate our Fourier-domain formulation. Finally, in Appendix B, we validate the results presented in Section 2, using an alternative derivation based on the Boussinesq–Papkovich potential.

2 ANALYTIC SOLUTION TO THE TRACTION BOUNDARY-VALUE PROBLEM IN A SEMI-INFINITE ELASTIC SOLID WITH GRAVITY

We wish to obtain an expression for the static deformation of a homogeneous elastic half space Ω subject to a distribution of traction $p_i(x_1, x_2)$ at its surface $x_3 = 0$. The surface $\partial\Omega$ is associated with the normal vector $n_i = -\delta_{i3}$, where δ_{ij} is the Kronecker's delta. The vertical displacement at the surface gives rise to a buoyancy restoring force so that the equilibrium holds (Wolf 1991; Johnston *et al.* 1998)

$$t_i = p_i + g_i, \quad (1)$$

where p_i is the applied surface traction,

$$g_i = \Delta\rho g u_3 n_i \quad (2)$$

is the pressure due to the assumed density contrast $\Delta\rho$ at the surface, and $t_i = \sigma_{ij} n_j$ is the resulting traction at the surface (Fig. 1). In terms of stress components we obtain the surface boundary condition

$$\begin{aligned} \sigma_{13}(x_1, x_2) &= -p_1(x_1, x_2), \\ \sigma_{23}(x_1, x_2) &= -p_2(x_1, x_2), \\ \sigma_{33}(x_1, x_2) &= -p_3(x_1, x_2) + \Delta\rho g u_3(x_1, x_2, 0), \end{aligned} \quad (3)$$

where σ_{ij} is the Cauchy stress tensor (Malvern 1969; Nemat-Nasser & Hori 1999). In the homogeneous elastic half-space, the conservation of linear momentum and Hooke's law give rise to the homogeneous Navier's equation

$$(\lambda + \mu)u_{j,ij} + \mu u_{i,jj} = 0, \quad (4)$$

where u_i is the vector-valued displacement field and λ and μ are the Lamé parameters. We look for a displacement field that satisfies the governing eq. (4) with boundary condition (1) at the surface and vanishing displacements at infinity.

Next we introduce the Galerkin vector potential and use it to solve two related subproblems: the Boussinesq's problem for the deformation due to normal loads at the surface, and the Cerruti's problem for the deformation due to tangential tractions at the surface. We consider a generalization of the classic formulation of the Cerruti's and Boussinesq's problems that includes a buoyancy restoring force at the surface. By applying the superposition theorem, we derive a general solution for the deformation in a half-space due to the application of some arbitrary tractions at the surface.

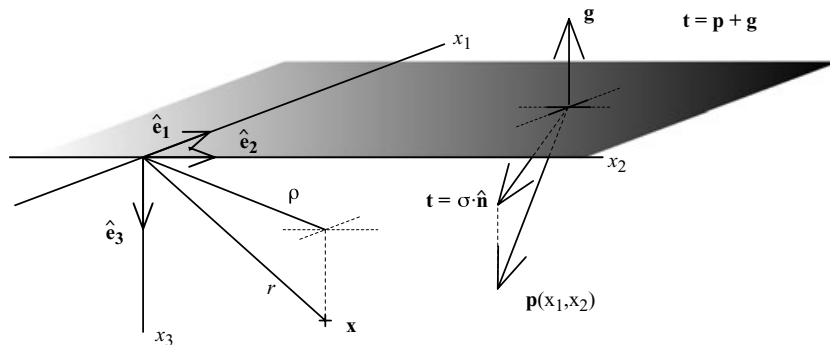


Figure 1. Geometry and boundary condition for the deformation due to arbitrary distributions of surface tractions. The surface traction $\mathbf{t}(\mathbf{x})$ is the sum of the applied load $\mathbf{p}(\mathbf{x})$ and the buoyancy restoring force $\mathbf{g} = \Delta\rho g u_3 \hat{\mathbf{n}}$. Displacement \mathbf{u} in the semi-infinite solid satisfies the homogeneous Navier's equation (4) with buoyancy condition (3).

2.1 The Galerkin vector potential

The Galerkin vector potential G_i (Westergaard 1935; Mindlin 1936b; Mindlin & Cheng 1950a; Steketee 1958) is defined by the change of variable

$$u_i = G_{i,jj} - \alpha G_{j,ij} \quad (5)$$

where the dimensionless constant α can be expressed in terms of the Lamé's parameters or Poisson's ratio

$$\alpha = \frac{\lambda + \mu}{\lambda + 2\mu} = \frac{1}{2(1 - \nu)}. \quad (6)$$

Inserting the Galerkin potential in the homogeneous Navier's equation (4) gives rise to

$$G_{i,jjkk} = 0. \quad (7)$$

In the absence of internal forces, the three Cartesian components G_i are biharmonic. By applying the 2-D horizontal (x_1, x_2) Fourier transforms

$$\begin{aligned} \hat{f}(k_1, k_2, x_3) &= \int_{-\infty}^{\infty} \int_{-\infty}^{\infty} f e^{-i2\pi(k_1x_1 + k_2x_2)} dx_1 dx_2, \\ f &= \int_{-\infty}^{\infty} \int_{-\infty}^{\infty} \hat{f}(k_1, k_2, x_3) e^{+i2\pi(k_1x_1 + k_2x_2)} dk_1 dk_2, \end{aligned} \quad (8)$$

where f is a scalar field and defining the angular wavenumbers $\omega_i = 2\pi k_i$ the biharmonic equation (7) simplifies to the fourth-order ordinary differential equation

$$\left(\frac{\partial^2}{\partial x_3^2} - \beta^2 \right)^2 G_i = 0, \quad (9)$$

where we have defined the radial angular velocity

$$\beta = (\omega_1^2 + \omega_2^2)^{1/2}. \quad (10)$$

A general solution for the component of the Galerkin vector is

$$\hat{G}_i = (A_i + B_i \beta x_3) e^{-\beta x_3} + (C_i + D_i \beta x_3) e^{+\beta x_3}. \quad (11)$$

Vanishing displacements at infinity ($x_3 \rightarrow \infty$) require $C_i = D_i = 0$, so that the general solution and its successive derivatives are

$$\begin{aligned} \hat{G}_i &= (A_i + B_i \beta x_3) e^{-\beta x_3}, \\ \hat{G}_{i,3} &= \beta (B_i - A_i - B_i \beta x_3) e^{-\beta x_3}, \\ \hat{G}_{i,33} &= \beta^2 (-2B_i + A_i + B_i \beta x_3) e^{-\beta x_3}, \\ \hat{G}_{i,333} &= \beta^3 (3B_i - A_i - B_i \beta x_3) e^{-\beta x_3}. \end{aligned} \quad (12)$$

The components of the stress tensor are, without loss of generality,

$$\begin{aligned} \sigma_{ij} &= \mu \left[(2\alpha - 1) \delta_{ij} G_{k,kl} \right. \\ &\quad \left. + G_{i,jkk} + G_{j,ikk} - 2\alpha G_{k,ijk} \right]. \end{aligned} \quad (13)$$

The semi-analytic solution in the Fourier domain for the deformation in a half space subject to surface traction is reduced to finding the values of the A_i and the B_i from the Fourier transform of the surface stresses, that is removing the six degrees of freedom in the Galerkin vector (12). Such a solution might be attainable by inverting a 6×6 square matrix, but this approach is not generally tractable. Instead, we solve independently the so-called Boussinesq's and Cerruti's problems, corresponding to the application of normal and tangential loads, respectively, at the surface of the half space, and obtain the full solution by linear superposition.

2.2 The Boussinesq's problem with gravity

The Boussinesq's problem arises from the application of a concentrated normal load $\mathbf{p} = p_3 \hat{\mathbf{e}}_3$ at the surface of the half-space. We consider an extended problem of an arbitrary distribution of normal tractions with buoyancy effects. The solution to this problem in the Fourier domain with no gravity was presented by Steketee (1958). Assuming that the first two components of the Galerkin vector potential can be set to zero, $G_1 = G_2 = 0$, we obtain from eqs (12) and (13) the shear stress components in the Fourier domain

$$\begin{aligned} \hat{\sigma}_{13} &= -2\mu i \omega_1 \beta^2 [(1 - 2\alpha)B_3 + \alpha(A_3 + B_3 \beta x_3)] e^{-\beta x_3}, \\ \hat{\sigma}_{23} &= -2\mu i \omega_2 \beta^2 [(1 - 2\alpha)B_3 + \alpha(A_3 + B_3 \beta x_3)] e^{-\beta x_3}, \end{aligned} \quad (14)$$

that both vanish identically at the surface if

$$A_3 = (2 - \alpha^{-1})B_3. \quad (15)$$

Combining the surface normal stress (derived from eqs 12 and 13)

$$\hat{\sigma}_{33} = 2\mu \alpha B_3 \beta^3 \quad (16)$$

and the vertical displacement at the surface (derived from eqs 5 and 12)

$$\hat{u}_3 = -\beta^2 B_3 \quad (17)$$

and using the boundary condition $\hat{\sigma}_{33} = -\hat{p}_3 + \Delta \rho g \hat{u}_3$ of eq. (1), one finds

$$B_3 = \frac{-\hat{p}_3}{2\mu \alpha \beta^2 (\beta + \Gamma)}, \quad (18)$$

where we have introduced the critical buoyancy wavenumber

$$\Gamma = \frac{\Delta \rho g}{2\mu \alpha} = (1 - \nu) \frac{\Delta \rho g}{\mu} \quad (19)$$

that represents the relative effect of gravity compared to the elastic rigidity. For a typical density contrast at the Earth's surface $\Delta \rho = 2.8 \times 10^3 \text{ kg m}^{-3}$ and shear modulus $G = 30 \text{ GPa}$, the associated critical wavelength is $\Gamma^{-1} \simeq 10^3 \text{ km}$. The solution for the displacement field for the Boussinesq's problem with the buoyancy effect is

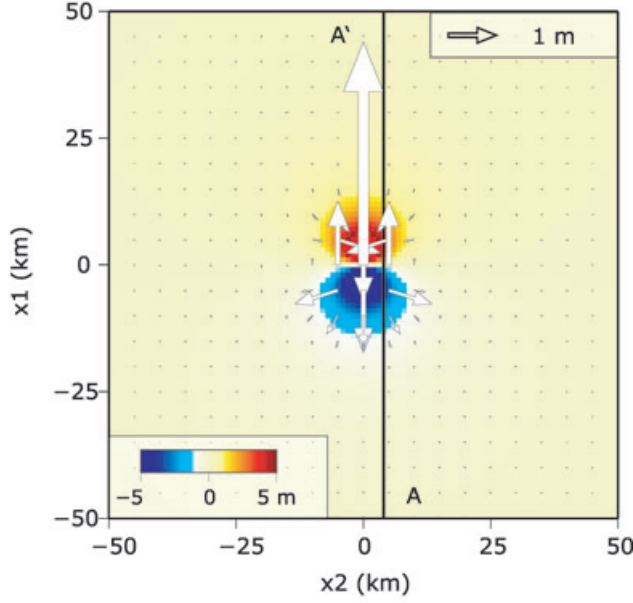
$$\begin{aligned} \hat{u}_1(k_1, k_2, x_3) &= i \alpha \omega_1 \beta B_3 [1 - \alpha^{-1} + \beta x_3] e^{-\beta x_3}, \\ \hat{u}_2(k_1, k_2, x_3) &= i \alpha \omega_2 \beta B_3 [1 - \alpha^{-1} + \beta x_3] e^{-\beta x_3}, \\ \hat{u}_3(k_1, k_2, x_3) &= -\alpha \beta^2 B_3 [\alpha^{-1} + \beta x_3] e^{-\beta x_3}. \end{aligned} \quad (20)$$

A comparison between the Fourier-domain solution (20) and the corresponding analytic solution using the space-domain Green's function (eq. A28 in Appendix A) is shown in Fig. 2 for the case of a moment load. We define a unit moment \mathbf{m}_{ij} as a force couple of equal and opposite magnitude $1/\epsilon$ in the $\hat{\mathbf{e}}_j$ direction separated by a distance ϵ in the $\hat{\mathbf{e}}_i$ direction. We compute the response of a moment load \mathbf{m}_{13} applied at the surface $x_3 = 0$ and compute the displacements at a depth of 3 km ignoring gravity ($\Gamma = 0$). The difference between the two fields is within a few percent of the maximum value. An elastic Green's function in the space domain that incorporates the effect of buoyancy is developed in Appendix A. The effect of gravity on viscoelastic relaxation following slip on a thrust fault is illustrated in a companion paper (B&F).

2.3 The Cerruti's problem with gravity

The Cerruti's problem corresponds to the deformation in a half-space due to the application of a tangential force at the surface. As there is no fundamental difference between applying forces in the

A. Fourier solution to the Boussinesq's problem



B. Comparison with analytic solution

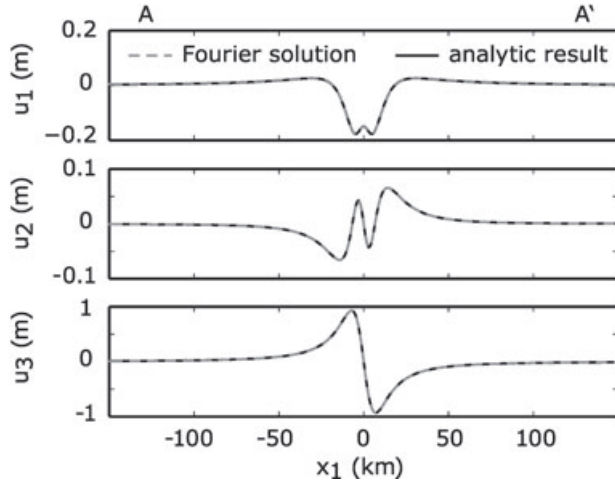


Figure 2. (A) Fourier-domain solution for the Boussinesq's problem (eq. 20). The map view corresponds to displacements at a depth of 3 km. The arrows indicate the horizontal displacement; the vertical displacement is shown by the colour. Upwards displacement is taken to be positive. A point-source moment \mathbf{m}_{13} is applied at the surface. (B) Comparison between the analytic solution and the semi-analytic Fourier domain solution along profile A–A'. These results correspond to a Poisson's solid ($\lambda = \mu$) without buoyancy effects at the surface ($\Gamma = 0$).

$\hat{\mathbf{e}}_1$ or the $\hat{\mathbf{e}}_2$ direction, we solve for deformation due to a distribution of forces applied in the $\hat{\mathbf{e}}_1$ direction only. A solution corresponding to the tangential forces oriented in the $\hat{\mathbf{e}}_2$ direction can be obtained by rotation about the x_3 axis. We therefore solve the homogeneous Navier's equation (4) considering the following boundary conditions: a prescribed surface stress σ_{13} , vanishing surface stress σ_{23} , equilibrium between the restoring buoyancy force and the normal stress σ_{33} and vanishing of displacements at infinity.

We start by using only one component of the Galerkin vector potential, such as $G_2 = G_3 = 0$. In the Fourier domain, we obtain

the stress components at the surface,

$$\begin{aligned}\hat{\sigma}_{13} &= 2\mu\beta[\alpha\omega_1^2 A_1 + (\beta^2 - \alpha\omega_1^2)B_1], \\ \hat{\sigma}_{23} &= 2\mu\alpha\omega_1\omega_2\beta[A_1 - B_1].\end{aligned}\quad (21)$$

From the surface boundary condition $\sigma_{23} = 0$, we obtain

$$A_1 = B_1 \quad (22)$$

and from the prescribed shearing stress in the $\hat{\mathbf{e}}_1$ direction we find

$$B_1 = \frac{-\hat{p}_1}{2\mu\beta^3}. \quad (23)$$

At this point, however, we have no vertical displacement at the surface and the condition of vanishing of normal stress at the surface is not satisfied. The Galerkin potential G_1 contributes to the surface normal stress

$$\hat{\sigma}_{33} = (\alpha - 1)\frac{i\omega_1\hat{p}_1}{\beta}. \quad (24)$$

This normal stress can be readily cancelled by application of the solution (20) to the Boussinesq's problem with the constant

$$B_3 = -i\omega_1\frac{1 - \alpha}{\alpha}\frac{B_1}{\beta + \Gamma}. \quad (25)$$

The solution to the Cerruti's problem requires two components of the Galerkin vector potential. Using eqs (22), (23) and (25) the solution displacement can be written

$$\begin{aligned}\hat{u}_1 &= B_1 \left\{ -2\beta^2 \right. \\ &\quad \left. + \frac{\omega_1^2}{1+h} \left[2 - \alpha^{-1} + \alpha h + (1 + \alpha h)\beta x_3 \right] \right\} e^{-\beta x_3}, \\ \hat{u}_2 &= \omega_1\omega_2\frac{B_1}{1+h} \left\{ 2 - \alpha^{-1} + \alpha h + (1 + \alpha h)\beta x_3 \right\} e^{-\beta x_3}, \\ \hat{u}_3 &= i\omega_1\beta\frac{B_1}{1+h} \left\{ \alpha^{-1} - 1 + (1 + \alpha h)\beta x_3 \right\} e^{-\beta x_3},\end{aligned}\quad (26)$$

where, for convenience, we have introduced a dimensionless parameter $h = \Gamma/\beta$. The solution to the Boussinesq's and Cerruti's problems can also be obtained analytically in the Fourier domain using the Boussinesq–Neuber–Papkovitch potential, as shown in Appendix B.

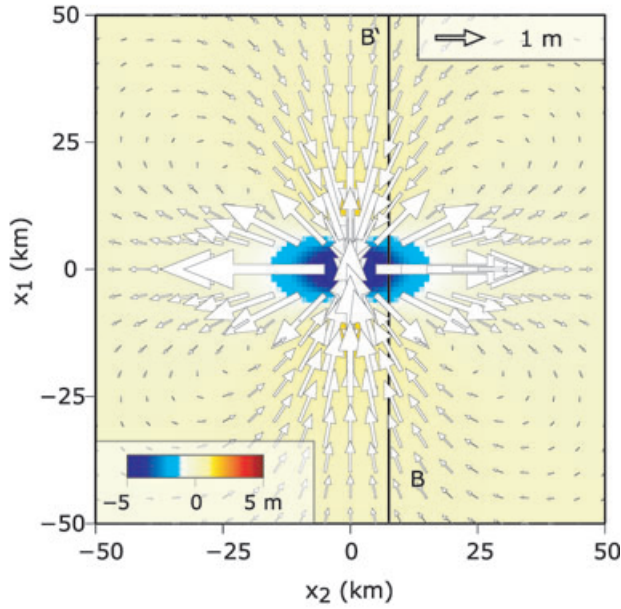
In case when the tangential traction is exerted in the $\hat{\mathbf{e}}_2$ direction, we have $\mathbf{p} = p_2\hat{\mathbf{e}}_2$, $B_1 = 0$, $B_2 = -\hat{p}_2/2\mu\beta^3$ and the displacement field is

$$\begin{aligned}\hat{u}_1 &= \omega_1\omega_2\frac{B_2}{1+h} \left\{ 2 - \alpha^{-1} + \alpha h + (1 + \alpha h)\beta x_3 \right\} e^{-\beta x_3}, \\ \hat{u}_2 &= B_2 \left\{ -2\beta^2 \right. \\ &\quad \left. + \frac{\omega_2^2}{1+h} \left[2 - \alpha^{-1} + \alpha h + (1 + \alpha h)\beta x_3 \right] \right\} e^{-\beta x_3}, \\ \hat{u}_3 &= i\omega_2\beta\frac{B_2}{1+h} \left\{ \alpha^{-1} - 1 + (1 + \alpha h)\beta x_3 \right\} e^{-\beta x_3}.\end{aligned}\quad (27)$$

The space-domain solution for the case of a tangential concentrated force on the plane boundary at the surface of a half-space is given by (Love 1927; Nemat-Nasser & Hori 1999)

$$\begin{aligned}u_1 &= \frac{1}{4\pi\mu r} \left[1 + \frac{x_1^2}{r^2} + (1 - 2\nu) \left(\frac{r}{r + x_3} - \frac{x_1^2}{(r + x_3)^2} \right) \right], \\ u_2 &= \frac{x_1 x_2}{4\pi\mu r} \left[\frac{1}{r^2} - \frac{1 - 2\nu}{(r + x_3)^2} \right], \\ u_3 &= \frac{x_1}{4\pi\mu r} \left[\frac{x_3}{r^2} + \frac{1 - 2\nu}{r + x_3} \right],\end{aligned}\quad (28)$$

A. Fourier solution to the Cerruti's problem



B. Comparison with analytic solution

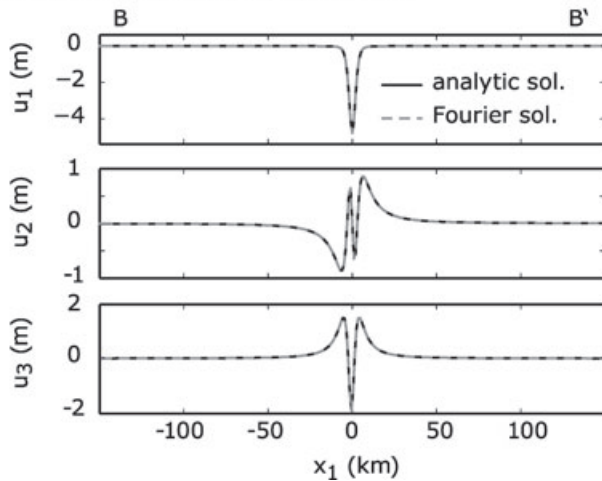


Figure 3. Benchmark of the Fourier-domain solution to the Cerruti's problem (eqs 26 and 27). (A) A point-source moment \mathbf{m}_{22} is applied at the surface of the half-space. The map view corresponds to displacements at a depth of 3 km. The arrows indicate the horizontal displacement; the vertical displacement is shown in colour. Vertical displacement is taken to be positive upwards. (B) Comparison between the analytic solution (eq. 28) and the semi-analytic Fourier-domain solution for the displacement along profile B–B'. In these calculations, we use a Poisson's solid ($\lambda = \mu$) and ignore the buoyancy effect ($\Gamma = 0$).

where $r = (x_1^2 + x_2^2 + x_3^2)^{1/2}$. We note a discrepancy in sign between the solutions given by Nemat-Nasser & Hori (1999) and Soutas-Little (1999) for the vertical component of displacement. Our results (eq. 28) agree with those of Soutas-Little (1999) and Okumura (1995). A comparison between the analytic solution (28) and the Fourier-domain formulation (26) is shown in Fig. 3. We apply a moment \mathbf{m}_{22} at the surface of the half-space and compute the solution on a plane at a depth of 3 km. Fig. 3(B) compares the analytic and numerical solutions along the horizontal profile B–B'. The error is less than 1 per cent of the maximum value for either displacement components.

2.4 Arbitrary distribution of surface traction with gravity

The general solution corresponding to the application of an arbitrary traction p_i at the surface of the half space is provided from the superposition of solutions to the Boussinesq's and Cerruti's problems. It makes use of the three components of the Galerkin vector potential. Combining results (20), (26) and (27) we obtain the complete displacement solution

$$\begin{aligned}\hat{u}_1 &= \left[-2B_1\beta^2 + \alpha\omega_1(B_1\omega_1 + B_2\omega_2)(1 + \beta x_3) \right. \\ &\quad \left. + \alpha i\omega_1\beta B_3(1 - \alpha^{-1} + \beta x_3) \right] e^{-\beta x_3}, \\ \hat{u}_2 &= \left[-2B_2\beta^2 + \alpha\omega_2(B_1\omega_1 + B_2\omega_2)(1 + \beta x_3) \right. \\ &\quad \left. + \alpha i\omega_2\beta B_3(1 - \alpha^{-1} + \beta x_3) \right] e^{-\beta x_3}, \\ \hat{u}_3 &= \alpha\beta^2 \left[i(\omega_1 B_1 + \omega_2 B_2)x_3 \right. \\ &\quad \left. - B_3(\alpha^{-1} + \beta x_3) \right] e^{-\beta x_3},\end{aligned}\quad (29)$$

where the constants B_i depend upon the applied traction

$$\begin{aligned}B_1 &= \frac{-\hat{p}_1}{2\mu\beta^3}, \\ B_2 &= \frac{-\hat{p}_2}{2\mu\beta^3}, \\ B_3 &= \frac{-\beta\hat{p}_3 + i(1 - \alpha)(\omega_1\hat{p}_1 + \omega_2\hat{p}_2)}{2\mu\alpha\beta^3(\beta + \Gamma)}.\end{aligned}\quad (30)$$

Formulation (29) is a closed-form solution in the horizontal Fourier domain to the traction boundary-value problem in a half space including a buoyancy restoring force at the surface. An equivalent expression can be found in the 3-D Fourier domain by forward Fourier transforming eq. (29) in the vertical direction

$$\begin{aligned}\hat{u}_1 &= \phi \left[-2B_1\beta^2 + \alpha\omega_1(B_1\omega_1 + B_2\omega_2)(1 - i\omega_3\phi) \right. \\ &\quad \left. + \alpha i\omega_1\beta B_3(1 - \alpha^{-1} - i\omega_3\phi) \right], \\ \hat{u}_2 &= \phi \left[-2B_2\beta^2 + \alpha\omega_2(B_1\omega_1 + B_2\omega_2)(1 - i\omega_3\phi) \right. \\ &\quad \left. + \alpha i\omega_2\beta B_3(1 - \alpha^{-1} - i\omega_3\phi) \right], \\ \hat{u}_3 &= \phi\alpha\beta \left[(\omega_1 B_1 + \omega_2 B_2)\omega_3\phi \right. \\ &\quad \left. - \beta B_3(\alpha^{-1} - i\omega_3\phi) \right],\end{aligned}\quad (31)$$

where we have defined

$$\phi = \frac{2\beta}{\omega_3^2 + \beta^2}.\quad (32)$$

3 A SEMI-ANALYTIC GREEN'S FUNCTION FOR THE ELASTIC HALF-SPACE UNDER GRAVITY

The elastic Green's function for a semi-infinite elastic solid with a free-surface boundary condition (Love 1927; Mindlin 1936a) provides the elementary solution that can be used to evaluate the 3-D deformation due to a distribution of point forces. As body force representations can be used to imitate dislocations (Burrige & Knopoff 1964; Steketee 1958), an elastic response of the crust due to slip of buried faults can be evaluated using the elastic Green's function (Okada 1992; Meade 2007). Both internal forces and surface tractions are required to represent slip on a fault if the latter intersects the surface (Backus & Mulcahy 1976a,b; Barbot *et al.* 2009b). An inhomogeneous traction boundary condition is also used in models of a heterogeneous crust (Barbot *et al.* 2009b). Finally, it can be required in models of time-dependent poroelastic relaxation (B&F).

Theoretically, the 3-D displacement field can be obtained with the convolution between the equivalent body force and the elastic Green's function (Love 1927; Mindlin 1936a). However, the forcing terms might occupy a large volume and the convolution in the space domain might not be computationally tractable. Our approach is to evaluate the elastic deformation numerically using a semi-analytic Green's function in the Fourier domain (Barbot *et al.* 2008a, 2009a,b). This approach takes advantage of the convolution theorem and the fast Fourier transform whereby the convolution becomes a product in the Fourier domain. The surface traction boundary condition is enforced using superposition. The Fourier-domain semi-analytic Green's function satisfying arbitrary surface traction boundary conditions can be used in multiple applications including elastostatic deformation in homogeneous and heterogeneous materials (Moulinec & Suquet 1998; Barbot *et al.* 2009b), models of fault creep (Barbot *et al.* 2009a) and other post-seismic post-seismic phenomena (see companion paper B&F).

3.1 A Fourier-domain elastic Green's function

Our approach to evaluate the 3-D displacement in a half-space due to an arbitrary distribution of body forces f_i subject to an inhomogeneous traction and buoyancy boundary condition is as follows. Consider the inhomogeneous Navier's equation

$$\mu \left(\frac{\alpha}{1-\alpha} u_{j,ij} + u_{i,jj} \right) + f_i = 0 \quad (33)$$

subject to the surface boundary condition

$$\sigma_{ij} n_j = q_i + \Delta \rho g u_3 n_i, \quad x_3 = 0, \quad (34)$$

where u_i is the vector-valued displacement field, σ_{ij} is the Cauchy stress tensor, $n_i = (0, 0, -1)$ is the surface normal vector and $q_i(x_1, x_2)$ is the prescribed load. The displacement that satisfies eqs (33) and (34) can be decomposed into a homogeneous and a particular contribution

$$u_i = u_i^h + u_i^p, \quad (35)$$

where the displacement field u_i^h is a solution to the homogeneous Navier's equation

$$\alpha u_{j,ij}^h + (1-\alpha) u_{i,jj}^h = 0, \quad (36)$$

with inhomogeneous surface boundary conditions and the particular solution u^p satisfies eq. (33) regardless of the surface boundary condition. The particular solution can be obtained in a straightforward manner in the Fourier domain. Upon Fourier transforming in the three directions eq. (33) becomes algebraic

$$\mu \left(\frac{\alpha}{1-\alpha} k_i k_j + k_l k_l \delta_{ij} \right) \hat{u}_j^p = \frac{1}{4\pi^2} \hat{f}_i, \quad (37)$$

where the k_i are the wavenumbers and the displacement field can be directly inverted to obtain

$$\hat{u}_i^p = \frac{1}{\mu} \frac{(1-\alpha) k_l k_l \delta_{ij} - \alpha k_i k_j}{4\pi^2 (k_l k_l)^2} \hat{f}_j, \quad (38)$$

where the hats correspond to the Fourier transform of the corresponding variables. We note that eq. (38) is ill-posed for $k_1 = k_2 = k_3 = 0$. The zero wavenumber component of the Fourier solution corresponds to a rigid-body displacement and does not involve an elastic deformation. We do not allow for a net displacement of the half space by setting $\hat{u}_i(0, 0, 0) = 0$. A particular solution to eq. (33) is provided by eq. (38) for any distribution of internal forces.

We now seek a homogeneous solution u^h such that the sum (35) satisfies the boundary condition (34). For convenience, as eq. (31) is already a Fourier-domain solution, we evaluate the surface tractions and the surface vertical displacements in the Fourier domain as well. A displacement field is associated with the stress

$$\sigma_{ij} = \mu \left(u_{i,j} + u_{j,i} - \frac{1-2\alpha}{1-\alpha} u_{k,k} \delta_{ij} \right) \quad (39)$$

and we define the surface traction due to the homogeneous and particular displacement fields by $t_i^h = \sigma_{ij}^h n_j$ and $t_i^p = \sigma_{ij}^p n_j$, respectively. In the Fourier domain, the stress can be written

$$\hat{\sigma}_{ij} = \mu i \left(\omega_j \delta_{il} + \omega_l \delta_{jl} - \frac{1-2\alpha}{1-\alpha} \omega_l \delta_{ij} \right) \hat{u}_l. \quad (40)$$

The contributions of vertical displacement \hat{u}_3^p and traction \hat{t}_i^p from the particular solution at the surface are, respectively,

$$\hat{u}_3^p(k_1, k_2, x_3 = 0) = \int_{-\infty}^{\infty} \hat{u}_3^p(k_1, k_2, k_3) dk_3 \quad (41)$$

and

$$\hat{t}_i^p(k_1, k_2) = \mu i \int_{-\infty}^{\infty} \left(\omega_j \hat{u}_i^p + \omega_l \hat{u}_j^p - \frac{1-2\alpha}{1-\alpha} \omega_l \hat{u}_l^p \delta_{ij} \right) n_j dk_3. \quad (42)$$

The solution to the homogeneous Navier's equation (36) is given by eq. (29), as discussed in Section 2. By definition of eq. (1), the traction and the surface vertical displacement of the homogeneous solution satisfy

$$t_i^h = p_i + \Delta \rho g u_3^h n_i \quad (43)$$

where the traction $p_i(x_1, x_2)$ is a degree of freedom required to satisfy eq. (34). We use linear superposition to cancel the contribution from the particular solution and satisfy the boundary condition (34). The displacements in the semi-infinite solid can be evaluated from a given applied traction $p_i(x_1, x_2)$ at the surface and the buoyancy boundary condition is automatically satisfied. We write

$$u^h = u^h(; p_i) \quad (44)$$

where we use the semi colon to denote the dependence of the homogeneous solution upon the prescribed boundary condition p_i at the surface. Using the decomposition (35) the boundary condition (34) can be written

$$t_i^h + t_i^p = q_i + \Delta \rho g (u_3^h + u_3^p) n_i \quad (45)$$

Using eq. (43) we constrain the last degree of freedom

$$p_i = -t_i^p + \Delta \rho g u_3^p n_i + q_i. \quad (46)$$

In the Fourier domain, the required homogeneous contribution is

$$\hat{u}^h = \hat{u}^h(; -\hat{t}_i^p + \Delta \rho g \hat{u}_3^p n_i + \hat{q}_i) \quad (47)$$

The displacement field due to a distribution of internal body forces and surface tractions is ultimately evaluated using the following steps. First, we apply a 3-D Fourier transform to the body-force field. Second, we apply the transfer function of eq. (38). We obtain a displacement field that satisfies periodic boundary conditions. The intermediate solution requires a correction to satisfy the traction boundary condition. We evaluate the 2-D traction field (46) in the Fourier domain by performing the integrals (41) and (42) numerically. We then evaluate a homogeneous solution that satisfies eq. (46) using the analytic solution (31). Summing the two displacement fields results in a solution that satisfies the inhomogeneous Navier's eq. (33) and the prescribed traction boundary condition (34). Finally, we perform a 3-D inverse Fourier transform numerically to obtain a displacement field in the space domain.

4 APPLICATIONS TO FAULTING AND VOLCANIC UNREST

We test the semi-analytic Green's function described in Section 3 against analytic results for the 3-D displacement due to fault slip and magmatic intrusions. Some benchmarks for strike-slip faults and a comparison with the numerical approach of Wang *et al.* (2003) are presented in Barbot *et al.* (2009a). Benchmarks for dip-slip faults in plane strain problems can be found in Barbot *et al.* (2009b). We start by comparing models of deformation for a point source using the solution of Mindlin & Cheng (1950a) for a nucleus of strain. We then describe models including sources of finite size and compare our numerical solution for strike-slip and dip-slip faults with the analytic solution of Okada (1992). Our formulation allows us to represent sources of arbitrary orientation and location in the half-space. We consider a case of a buried thrust fault as an example.

4.1 Point of dilatation

First, we consider the case of a dilatation source. A point source of dilatation is an approximation representing isometric magmatic intrusions subject to a pressure boundary condition (Mogi 1958). The surface displacement (at $x_3 = 0$) due to a source of dilatation at depth y_3 in a semi-infinite solid with Poisson's ratio ν is (Mindlin & Cheng 1950a,b)

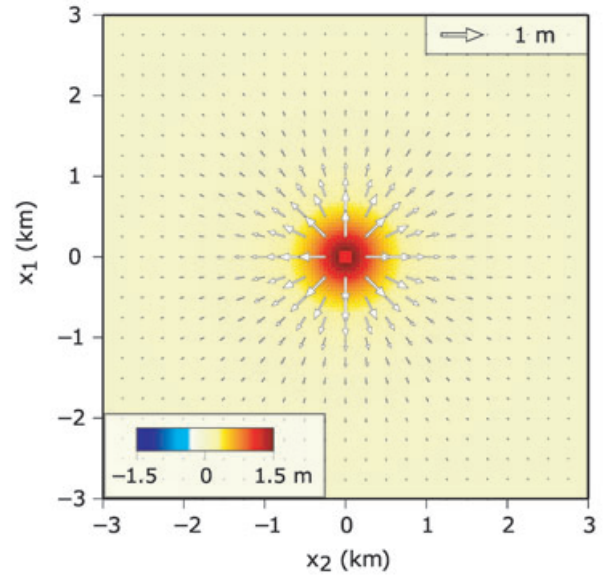
$$\begin{aligned} u_1 &= + \frac{1 + \nu}{\pi} \frac{x_1}{r^3}, \\ u_2 &= + \frac{1 + \nu}{\pi} \frac{x_2}{r^3}, \\ u_3 &= - \frac{1 + \nu}{\pi} \frac{y_3}{r^3}, \end{aligned} \quad (48)$$

where $r = (x_1^2 + x_2^2 + y_3^2)^{1/2}$ is the distance from the source centred at the origin and an observation point at the surface (Fig. 1). The dilatation source of eq. (48) can be represented by the eigenstrain $\epsilon_{ij}^i = \delta_{ij}$, a moment density $m_{ij} = 3\kappa \delta_{ij}$ and an equivalent body force $f_i = -m_{ij,j}$ in the notation of Barbot *et al.* (2009a,b) and Barbot & Fialko (2010, submitted), where κ is the bulk modulus. Our numerical solution for the surface displacement is shown in Fig. 4(A) for a point source at depth $y_3 = 0.5$ km. In Fig. 4(B), we show the numerical error as a function of the number of nodes in our 3-D grid. We normalize the sum of the square of the residuals between the semi-analytic and the analytic solution of eq. (48) by the norm of the analytic signal. In these calculations we use a Poisson's solid ($\lambda = \mu$ and $\nu = 1/4$), ignore the density contrast at the surface ($\Gamma = 0$) and use a uniform sampling size of $\Delta x_i = 0.05$ km. A simulation using the 512^3 nodes takes about 30 s on a four-cpu shared-memory computer. The error decays to less than 1 per cent for large computational grids where the effect of periodicity is smaller. Calculations with different values of Poisson's ratio gave rise to similar residuals.

4.2 Finite fault deformation

We now consider the case of finite faults. We model finite faults with a distribution of internal forces and surface traction (Barbot *et al.* 2009a). Fig. 5(A) (left panel) shows the surface displacements due to a vertical left-lateral strike-slip fault with a slip of 1 m. The right panel shows the residuals between our numerical solution and the analytic formulation of Okada (1992). The residuals at the tip of the fault are due to our tapering of the slip at the edges of the fault. We taper slip at the fault tips to mitigate a possible Gibbs

A. Surface displacement for a buried dilatation source



B. Numerical error

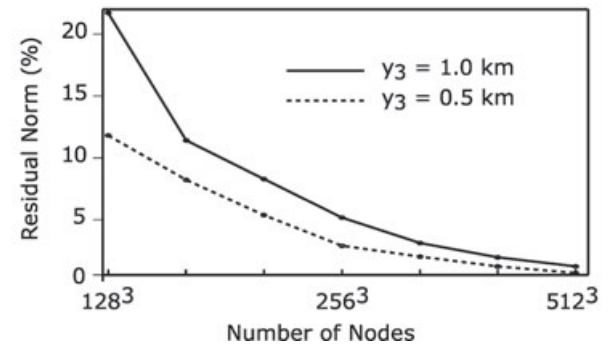
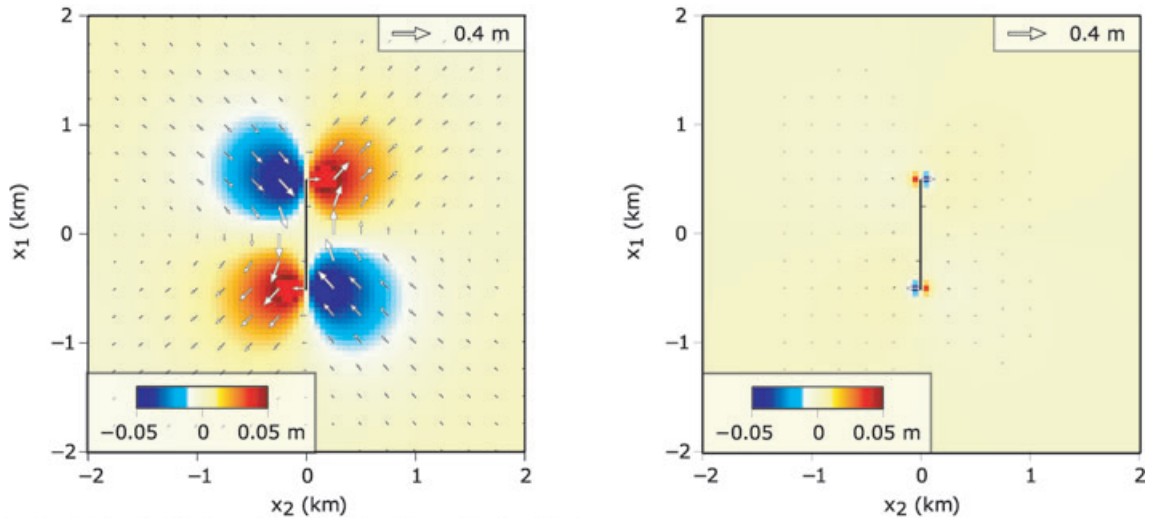


Figure 4. (A) Map view of surface displacement due to a dilatation source centered at $y_1 = y_2 = 0$ and buried at a depth of $y_3 = 0.5$ km. Horizontal and vertical components of displacement are represented by the vectors and the colour, respectively. Uplift is taken to be positive. (B) The norm of the residuals between the numerical solution and the formulation of Mindlin & Cheng (1950b) as a function of the number of nodes in the 3-D grid for a uniform isotropic sampling of $\Delta x_i = 0.05$ km. The error is normalized by the norm of the analytic solution. The dashed and solid-line profiles correspond to a dilatation source at depth of $y_3 = 0.5$ and 1.0 km, respectively. The numerical error decreases as the boundaries of the computational domain increases and the non-desired effect of periodicity decreases.

phenomenon (Barbot *et al.* 2008a); also the tapered slip distribution is more physically reasonable than the constant slip (Fialko 2004, 2007). Fig. 5(B) shows the surface displacements associated with a vertical dip-slip fault with a 1 m slip on a plane extending from the surface to a depth of 1 km. Models of dip-slip faults intersecting the surface require both equivalent body forces and equivalent surface traction to represent the slip discontinuity. The residuals with the solution of Okada (1992) are localized near the fault and arise from the displacement discontinuity, which cannot be accurately sampled by a continuous field down to a scale of numerical discretization. For both the strike-slip and dip-slip faults, the residuals immediately away from the fault discontinuity fall below 5 per cent of the exact solution.

Finally, we use the proposed semi-analytic Green's function to compute the displacement due to a thrust fault. Fig. 6(A) shows

A. Strike-slip fault surface displacement and residuals with the solution of Okada (1992)



B. Vertical dip-slip fault and residuals with analytic solution

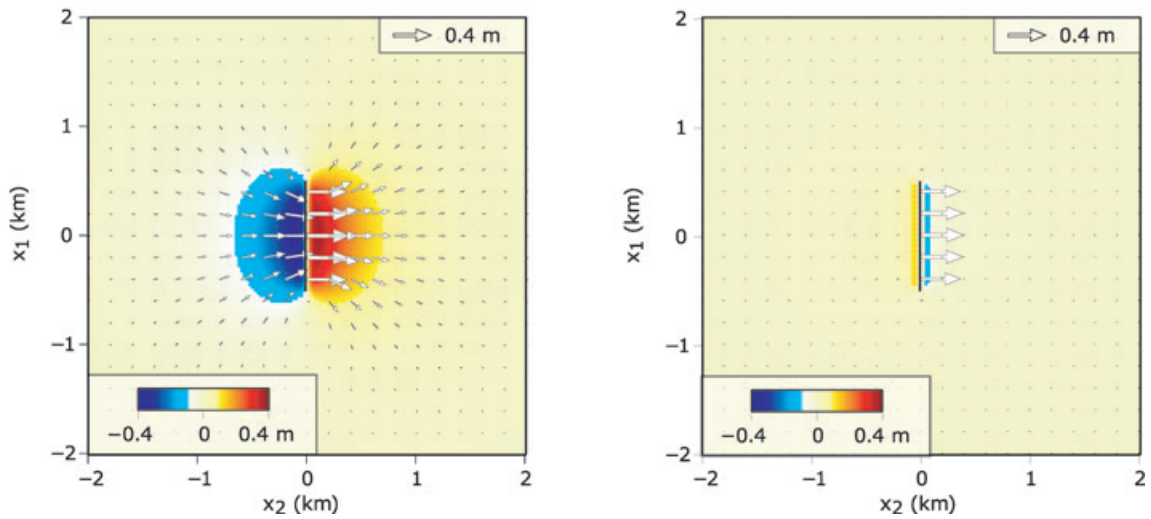


Figure 5. (A) Map view of surface displacement due a vertical, 1 km long, strike-slip fault extending from the surface to a depth of 1 km with a 1 m slip (left panel) and residuals with the analytic solution of Okada (1992) (right panel). (B) Surface displacements due to a 1 m slip on a vertical dip-slip fault with same dimensions as in A). The fault trace is indicated by a solid black line. A dip-slip fault intersecting the surface is modelled with both internal body forces and surface traction. Residuals in (A) are due to the tapering of the fault tip; residuals in (B) come from the problem of sampling a displacement field that is not single-valued at the fault.

the displacement field at the surface due to a buried thrust fault 10-km long and 10-km wide in the down-dip direction. The top of the fault is buried at a depth of 5 km. The residuals with the analytic solution of Okada (1992) are shown in Fig. 6(B) (note the change of scale). Overall, residuals are about 2 per cent of the expected signal. The biggest residuals are located near the top of the fault and are due to slip tapering of the fault tips in our model. We investigate the effect of sampling and size of the computational domain on the numerical solution accuracy. Fig. 6(C) shows the norm of the residuals as a function of the number of nodes in the computational grid for two different sampling size. For small grids, the error is greater for small sampling size. Fig. 6(C) shows that the error corresponding to using a grid with linear dimension 12.8 km is comparable to the error arising from using a grid with the same linear dimension but doubled number of nodes. We conclude that a primary source of error in this case comes from the distance to the periodic boundary. For larger computational grids, residuals associated with a denser sampling become smaller, illustrating the

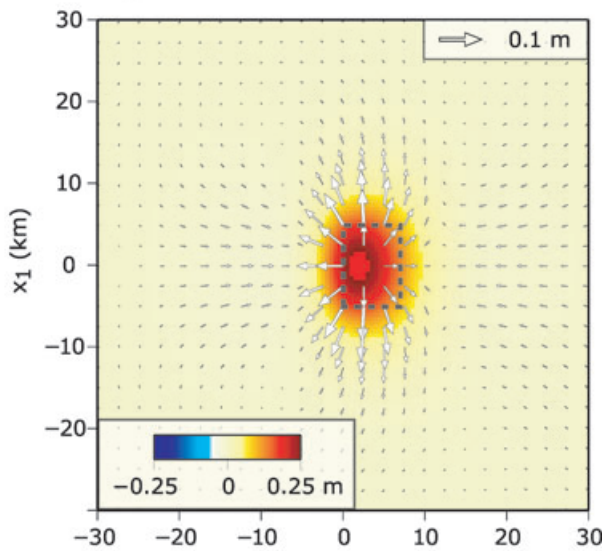
tradeoffs between the requirement of large computational domains and small discretization. We performed additional tests for a buried dip-slip fault, varying the dip angle from 0° to 90° and the fault length between 10 and 30 km, all other parameters being otherwise the same. We found similar good agreements between numerical and analytic solutions as in the example shown in Fig. 6.

4.3 Modelling heterogeneous properties of crustal rocks

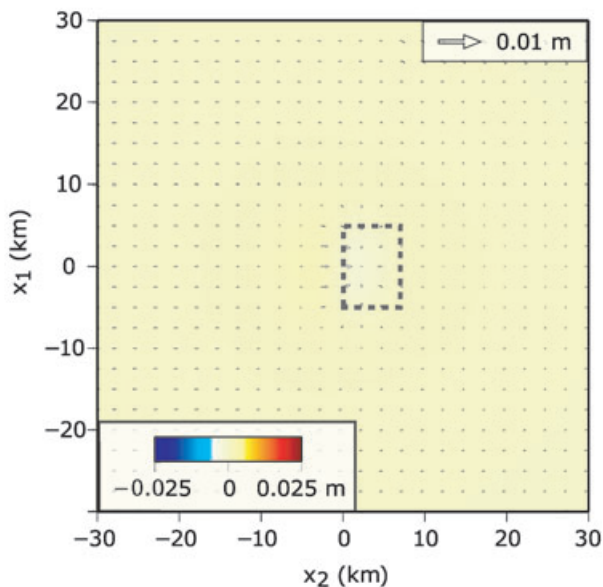
The homogeneous elastic Green's function can be used to model elastic deformation in a heterogeneous half-space by means of a homogenization method (Du *et al.* 1997; Cochran *et al.* 2009; Barbot *et al.* 2009b). Successive approximations $u^{(n+1)}$ of the displacement field can be obtained with the convolution between the homogeneous Green's function and the body forces

$$f_i^{(n)} = -(C'_{ijkl}u_{k,l})_{,j} \quad (49)$$

A. Surface displacement for a thrust fault



B. Residuals with the solution of Okada (1992)



C. Numerical error

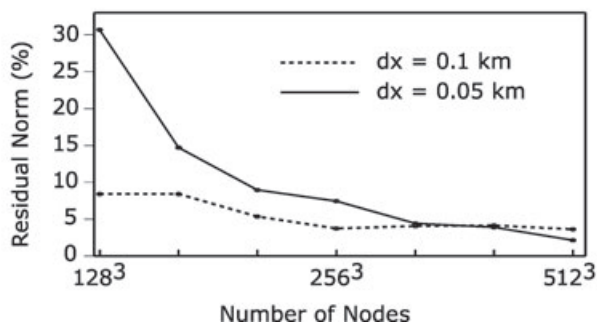


Figure 6. (A) Map view of surface displacement due a 45°-dip, 10-km long, 10-km wide (in down-dip direction) thrust fault buried at a depth of 5 km (dashed rectangle). (B) Residuals with the analytic solution of Okada (1992). (C) The norm of the residuals as a function of the number of nodes in the 3-D grid.

and the surface tractions

$$t_i^{(n)} = C'_{ijkl} u_{k,j}^{(n)} n_j \quad (50)$$

starting from an initial guess displacement field $u^{(0)}$, where superscript (n) is the iteration number and C'_{ijkl} is the elastic tensor deviation from an arbitrary background value.

Fig. 7 shows an application for the case of a vertical dip-slip rupture in the vicinity of an infinitely long compliant zone. The fault extends from the surface to a depth $W = 10$ km, is $2W$ long in the strike direction and slips 1 m uniformly. The bulk modulus is uniform in the half-space and the compliant zone, also extending from the surface to a depth W , is characterized by a thickness $T = W/5$ and a 10 per cent reduction in shear modulus. The displacement anomaly originating from the compliant zone exhibits additional uplift to the East of the rupture where the shear modulus is reduced (Fig. 7B). We performed a similar calculation using a finite-element method using the Simulia software (formally Abaqus, www.simulia.com). The small residuals (Fig. 7C) between the two simulations indicate a very good accuracy of our Fourier-domain Green's function used in combination with the homogenization method.

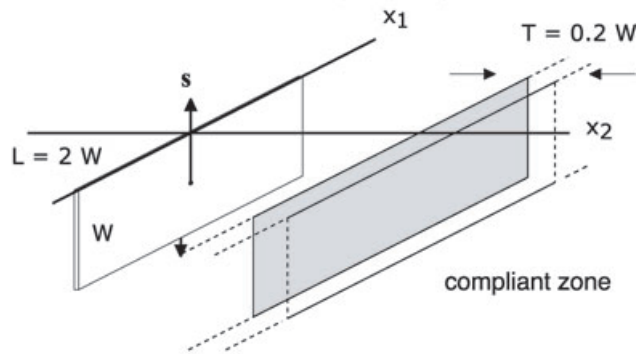
Figs 4, 5 and 6 illustrate simple sources of deformation. Complex geometries can be readily accounted for in our method using a superposition of such elementary sources (Barbot *et al.* 2009a,b). We conclude that the proposed Fourier-domain semi-analytic Green's function approach is sufficiently accurate and flexible to allow realistic simulations of crustal deformation due to earthquake- and volcano-related phenomena.

5 CONCLUSIONS

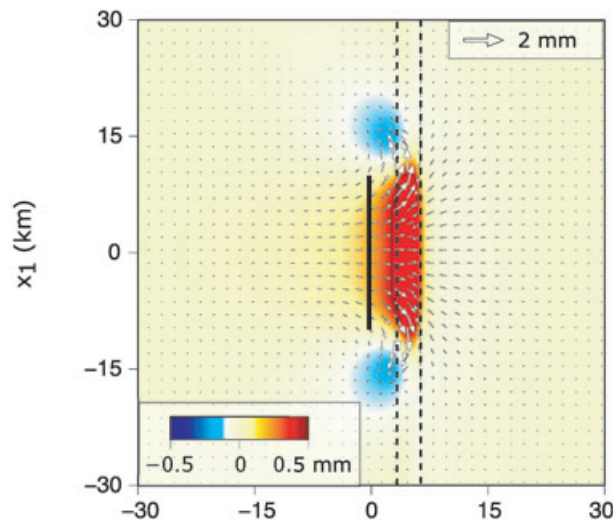
Building on the classic work of Steketee (1958), we derived the analytic Fourier-domain solution for displacements due to an arbitrary distribution of tangential and normal loads at the surface of a semi-infinite solid. Our formulation generalizes the so-called Boussinesq's and Cerruti's problems by accounting for the effect of buoyancy at the surface due to a large density contrast between the lithosphere and the atmosphere. The buoyancy boundary condition is an approximation to the full effect of gravity where self-gravitation and internal density variations are ignored. The full Fourier-domain solution with surface buoyancy is given by eq. (29). We note that the solution of eq. (29) can be found using the Galerkin as well as using the Boussinesq–Papkovitch–Neuber vector potentials (Appendix B). We also derived a space-domain Green's function for the deformation due to the application of normal loads at the surface of the half space with a buoyancy boundary condition (Appendix A). We use a perturbation approach, assuming that the effect of gravity is a small contribution to the deformation, to approximate a solution for the elastic Green's function. The accuracy of our solution is validated by a good agreement between the Fourier and space-domain solutions to the generalized Boussinesq's problem.

Numerous problems of elastic deformation due to internal forces and surface traction come about from static models of faulting and from time-dependent models of postseismic relaxation (Barbot *et al.* 2009b), Barbot & Fialko (2010, submitted). The displacement or velocity can theoretically be obtained by the convolution in the space domain between the elastic Green's function and the body force, however this is not always practical because the internal forces can be distributed over a larger domain and the convolution operation scales as N^2 , where N is the number of nodes in the simulation. We derived an efficient way to evaluate the 3-D deformation in a half-space due to the presence of an arbitrary distribution of internal forces and surface tractions. Our method involves (1) obtaining

A. Fault and compliant zone geometry



B. Elastic structure contribution



C. Residuals with finite-element calculations

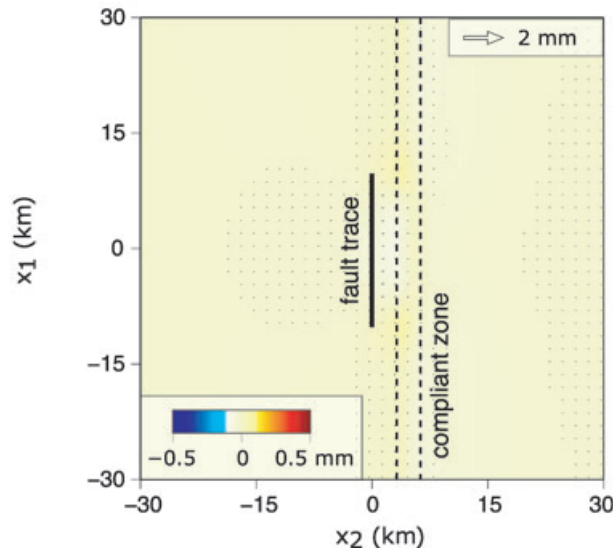


Figure 7. (A) Geometry of the finite dip-slip fault and the infinitely long compliant zone. (B) Map view of displacement anomalies—compared to the prediction of homogeneous elasticity—due to the presence of a compliant zone surrounding a dip-slip fault. (C) Residuals with a similar calculation using a finite element method (FEM).

the displacement field in a periodic full space due to the same internal forces and (2) adding a homogeneous solution to satisfy the prescribed boundary condition, including the buoyancy effect. The periodic solution can be readily obtained in the Fourier domain and the auxiliary analytic homogeneous solution is given by eq. (29). The two-step method is computationally efficient and easily parallelized to deal with large computational grids. The semi-analytic solution compares well to analytic solutions for the displacement field due to strike-slip and dip-slip faults of arbitrary orientation and point-sources of dilatation, within a typical maximum error of 5 per cent for the explored range of model sizes. Our Fourier-domain solution can be efficiently used to model elastostatic deformation (Barbot *et al.* 2009b), as well as quasi-static deformation such as that due to the most common postseismic mechanisms (viscoelastic relaxation, poroelastic rebound and fault creep). Application of the proposed Green's function to models of time-dependent postseismic deformation are considered in a companion paper (B&F).

ACKNOWLEDGMENTS

A numerical code used in this paper is available at <http://sylvain.barbot.free.fr/crust/>. The manuscript benefited from the comments of the Editor Massimo Cocco, and the thorough reviews of three anonymous reviewers. This work was supported by the National Science Foundation (grant EAR-0944336) and the Southern California Earthquake Center (the SCEC contribution number for this paper is 1335).

REFERENCES

- Backus, G. & Mulcahy, M., 1976a. Moment tensors and other phenomenological descriptions of seismic sources—I. Continuous displacements, *Geophys. J. R. astr. Soc.*, **46**, 341–361.
- Backus, G. & Mulcahy, M., 1976b. Moment tensors and other phenomenological descriptions of seismic sources—II. Discontinuous displacements, *Geophys. J. R. astr. Soc.*, **47**, 301–329.
- Barbot, S. & Fialko, Y., 2010. A unified continuum representation of postseismic relaxation mechanisms: semi-analytic models of afterslip, poroelastic rebound and viscoelastic flow, *Geophys. J. Int.*, in press, doi:10.1111/j.1365-246X.2010.04678.x.
- Barbot, S., Fialko, Y. & Sandwell, D., 2008a. Effect of a compliant fault zone on the inferred earthquake slip distribution, *J. geophys. Res.*, **113**(B6), doi:10.1029/2007JB005256.
- Barbot, S., Hamiel, Y. & Fialko, Y., 2008b. Space geodetic investigation of the coseismic and postseismic deformation due to the 2003 Mw 7.2 Altai earthquake: implications for the local lithospheric rheology, *J. geophys. Res.*, **113**, B03403, doi:10.1029/2007JB005063.
- Barbot, S., Fialko, Y. & Bock, Y., 2009a. Postseismic deformation due to the Mw 6.0 2004 Parkfield earthquake: stress-driven creep on a fault with spatially variable rate-and-state friction parameters, *J. geophys. Res.*, **114**, B07405, doi:10.1029/2008JB005748.
- Barbot, S., Fialko, Y. & Sandwell, D., 2009b. Three-dimensional models of elasto-static deformation in heterogeneous media, with applications to the Eastern California Shear Zone, *Geophys. J. Int.*, **179**(1), 500–520.
- Bender, C.M. & Orszag, S.A., 1978. *Advanced Mathematical Methods for Scientists and Engineers*, McGraw-Hill, New York.
- Burridge, R. & Knopoff, L., 1964. Body force equivalents for seismic dislocations, *Bull. seism. Soc. Am.*, **54**(6), 1875–1888.
- Cochran, Y., Li, Y.-G., Shearer, P., Barbot, S., Fialko, Y. & Vidale, J., 2009. Seismic and geodetic evidence for extensive, long-lived fault damage zones, *Geology*, **37**(4), 315–318.
- Du, Y., Segall, P. & Gao, H., 1997. Quasi-static dislocations in three-dimensional inhomogeneous media, *Geophys. Res. Lett.*, **24**(18), 2347–2350.

- Fialko, Y., 2004. Probing the mechanical properties of seismically active crust with space geodesy: study of the co-seismic deformation due to the 1992 M_w 7.3 Landers (Southern California) earthquake, *J. geophys. Res.*, **109**, B03307, doi:10.1029/2003JB002756.
- Fialko, Y., 2006. Interseismic strain accumulation and the earthquake potential on the southern San Andreas fault system, *Nature*, **441**, 968–971.
- Fialko, Y., 2007. Fracture and frictional mechanics—theory, in *Treatise on Geophysics*, Vol. 4, pp. 83–106, ed. Schubert, G., Elsevier Ltd., Oxford.
- Fialko, Y., Khazan, Y. & Simons, M., 2001a. Deformation due to a pressurized horizontal circular crack in an elastic half-space, with applications to volcano geodesy, *Geophys. J. Int.*, **146**, 181–190.
- Fialko, Y., Simons, M. & Agnew, D., 2001b. The complete (3-D) surface displacement field in the epicentral area of the 1999 M_w 7.1 Hector Mine earthquake, southern California, from space geodetic observations, *Geophys. Res. Lett.*, **28**, 3063–3066.
- Freed, A.M. & Bürgmann, R., 2004. Evidence of power-law flow in the Mojave desert mantle, *Nature*, **430**, 548–551.
- Hsu, Y.-J. *et al.*, 2006. Friction afterslip following the 2005 Nias-Simeuleu earthquake, Sumatra, *Science*, **312**, 1921–1926.
- Johnston, P., Wu, P. & Lambeck, K., 1998. Dependence of horizontal stress magnitude on load dimension in glacial rebound models, *Geophys. J. Int.*, **132**, 41–60.
- Love, A.E.H., 1927. *A Treatise on the Mathematical Theory of Elasticity*, Cambridge University Press, Cambridge, reprinted in 1944 by Dover Publications, New York.
- Malvern, L.E., 1969. *Introduction to the Mechanics of a Continuum Medium*, 713 pp., Prentice-Hall, Englewood Cliffs, NJ.
- McGuire, J.J. & Segall, P., 2003. Imaging of seismic fault slip transients recorded by dense geodetic networks, *Geophys. J. Int.*, **155**, 778–788.
- Meade, B.J., 2007. Algorithms for the calculation of exact displacements, strains, and stresses for triangular dislocation elements in a uniform elastic half space, *Comp. Geosci.*, **33**(8), 1064–1075.
- Mindlin, R.D., 1936a. Force at a point in the interior of a semi-infinite solid, *J. Appl. Phys.*, **7**, 195–202.
- Mindlin, R.D., 1936b. Note on the Galerkin and Papkovitch stress functions, *Bull. Am. Math. Soc.*, **42**(6), 373–376, doi:10.1090/S0002-9904-1936-06304-4.
- Mindlin, R.D. & Cheng, D.H., 1950a. Nuclei of strain in the semi-infinite solid, *J. Appl. Phys.*, **21**, 926–930, doi:10.1063/1.1699785.
- Mindlin, R.D. & Cheng, D.H., 1950b. Thermoelastic stress in the semi-infinite solid, *J. Appl. Phys.*, **21**, 931–933.
- Miyazaki, S., McGuire, J.J. & Segall, P., 2003. A transient subduction zone slip episode in southwest Japan observed by the nationwide GPS array, *J. geophys. Res.*, **108**(B2), doi:10.1029/2001JB000456.
- Mogi, K., 1958. Relations between the eruptions of various volcanoes and the deformations of the ground surfaces around them, *Bull. Earthquake Res. Inst. Univ. Tokyo*, **36**, 99–134.
- Moulinec, H. & Suquet, P., 1998. A numerical method for computing the overall response of nonlinear composites with complex microstructure, *Comp. Meth. App. Mech. Eng.*, **157**, 69–94, 1998.
- Nemat-Nasser, S. & Hori, M., 1999. *Micromechanics: Overall Properties of Heterogeneous Materials*, 2nd edn, Elsevier, Amsterdam.
- Nguyen, T.-K., Sab, K. & Bonnet, G., 2008. Green's operator for a periodic medium with traction-free boundary conditions and computation of the effective properties of thin plates, *Int. J. Sol. Struct.*, **45**, 6518–6534, doi:10.1016/j.ijsolstr.2008.08.015.
- Okada, Y., 1992. Internal deformation due to shear and tensile faults in a half-space, *Bull. seism. Soc. Am.*, **82**, 1018–1040.
- Okumura, I.A., 1995. On the generalization of Cerruti's problem in an elastic half-space, *Proc. Japan Soc. Civ. Eng.*, **519**, 1–32.
- Pearse, J. & Fialko, Y., 2010. Mechanics of active magmatic intraplate in the Rio Grande Rift near Socorro, New Mexico, *J. geophys. Res.*, in press, doi:10.1029/2009JB006592.
- Pollitz, F.F., 1997. Gravitational viscoelastic postseismic relaxation on a layered spherical Earth, *J. geophys. Res.*, **102**, 17 921–17 941.
- Pollitz, F.F., Wicks, C. & Thatcher, W., 2001. Mantle flow beneath a continental strike-slip fault: postseismic deformation after the 1999 Hector Mine earthquake, *Science*, **293**, 1814–1818.
- Reid, H.F., 1910. The Mechanics of the Earthquake, *The California Earthquake of April 18, 1906*, Vol. 2, Carnegie Institution of Washington, Washington, DC.
- Rundle, J.B., 1982. Viscoelastic-gravitational deformation by a rectangular thrust fault in a layered earth, *J. geophys. Res.*, **87**(B9), 7787–7796.
- Savage, J., 1974. Dislocations in seismology, in *Dislocations Theory: A Treatise*, ed. Nabarro, F., Marcel Dekker, New York.
- Simons, M., Fialko, Y. & Rivera, L., 2002. Coseismic deformation from the 1999 M_w 7.1 Hector Mine, California, earthquake, as inferred from InSAR and GPS observations, *Bull. seism. Soc. Am.*, **92**, 1390–1402.
- Smith, B. & Sandwell, D., 2004. A three-dimensional semianalytic viscoelastic model for time-dependent analyses of the earthquake cycle, *J. geophys. Res.*, **109**, B12401, doi:10.1029/2004JB003185.
- Soutas-Little, R.W., 1999. *Elasticity*, Courier Dover Publications.
- Steketee, J.A., 1958. On Volterra's dislocations in a semi-infinite elastic medium, *Can. J. Phys.*, **36**, 192–205.
- Wang, R., Martin, F. & Roth, F., 2003. Computation of deformation induced by earthquakes in a multi-layered elastic crust - FORTRAN programs EDGRN/EDCMP, *Comp. Geosci.*, **29**, 195–207.
- Wang, R., Lorenzo-Martin, F. & Roth, F., 2006. PSGRN/PSCMP—a new code for calculating co- and post-seismic deformation, geoid and gravity changes based on the viscoelastic-gravitational dislocation theory, *Comp. Geosci.*, **32**, 527–541.
- Westergaard, H.M., 1935. General solution of the problem of elastostatics of an n -dimensional homogeneous isotropic solid in an n -dimensional space, *Bull. Am. Math. Soc.*, **41**(10), 695–699, doi:10.1090/S0002-9904-1935-06178-6.
- Wolf, D., 1991. Viscoelastodynamics and of a stratified, compressible planet: incremental field equations and shot- and long-time asymptotes, *Geophys. J. Int.*, **104**, 401–417.
- Yang, X.-M., Davis, P.M. & Dieterich, J.H., 1988. Deformation from inflation of a dipping finite prolate spheroid in an elastic half-space as a model for volcanic stressing, *J. geophys. Res.*, **93**, 4249–4257.

APPENDIX A: SPACE-DOMAIN ANALYTIC GREEN'S FUNCTION WITH BUOYANCY BOUNDARY CONDITION

In this appendix, we derive an analytic solution for the elastic Green's function for the case of the application of a concentrated normal load at the surface of a semi-infinite elastic body. Our solution extends the classic solution to the Boussinesq's problem (Love 1927; Nemat-Nasser & Hori 1999) to a generalized boundary condition where surface normal displacement is counteracted by a buoyancy force. We use the analytic solution derived in this Appendix to validate the Fourier-domain solution shown in Section 2. We first introduce the Boussinesq–Papkovitch–Neuber vector potential, then use this potential to solve for the elastic Green's function with buoyancy boundary condition. Our solution of eq. (A27) is obtained using the perturbation method where we assume that the buoyancy effect is a small contribution to the total deformation.

A1 The Boussinesq–Papkovitch–Neuber potential

The Boussinesq–Papkovitch–Neuber representation (Mindlin 1936b) comes about when applying the Helmholtz decomposition to the solution to the Navier's equation (4) as follows:

$$u_i = \phi_{,i} + \epsilon_{ijk} A_{j,k} \quad \text{with} \quad A_{j,j} = 0, \quad (\text{A1})$$

where ϕ and A_i are scalar and vector potentials, respectively, and ϵ_{ijk} is the Levi–Civita symbol. In the absence of body forces the conservation of momentum gives rise to

$$[\phi_{,i} + (1 - \alpha)\epsilon_{ijk} A_{j,k}]_{,jj} = 0, \quad (\text{A2})$$

where we denoted

$$\alpha = \frac{\lambda + \mu}{\lambda + 2\mu} = \frac{1}{2(1 - \nu)}. \quad (\text{A3})$$

Defining the harmonic vector potential

$$B_i = \frac{1}{1 - \alpha} \phi_{,i} + \epsilon_{ijk} A_{j,k} \quad (\text{A4})$$

and its divergence

$$B_{j,j} = \frac{\alpha}{1 - \alpha} \phi_{,jj} \quad (\text{A5})$$

one obtains, without loss of generality,

$$\phi = \frac{1 - \alpha}{2} (x_k B_k + B_0), \quad (\text{A6})$$

where we have used the vector identity $(x_k B_k)_{,ij} = 2 B_{j,j}$ and defined B_0 as a harmonic scalar. From the definition of B_i , we have

$$\epsilon_{ijk} A_{j,k} = B_i - \frac{1}{1 - \alpha} \phi_{,i}. \quad (\text{A7})$$

By combining expressions (A1), (A4), (A6) and (A7), one obtains the following representation:

$$u_i = B_i - \frac{\alpha}{2} [x_k B_k + B_0]_{,i}. \quad (\text{A8})$$

This is the Papkovitch–Neuber elastic potential, which represents the solution to the Navier’s equation in the absence of body force in terms of a harmonic vector B_i and a harmonic scalar B_0 . Without loss of generality, one has the following results

$$\begin{aligned} u_{j,j} &= (1 - \alpha) B_{j,j}, \\ \frac{1}{\mu} \sigma_{ij} &= (2\alpha - 1) \delta_{ij} B_{k,k} + B_{i,j} + B_{j,i} \\ &\quad - \alpha (x_k B_k + B_0)_{,ij}. \end{aligned} \quad (\text{A9})$$

The advantage of the Papkovitch–Neuber potential is that it may allow one to obtain an analytic solution to the Navier’s equation in an easier way by manipulating harmonic vector and scalar potentials.

A2 The Boussinesq’s problem with buoyancy surface boundary conditions in the space domain

We look for an analytic expression of the Green’s function representing the displacement field experienced by the homogeneous elastic half-space Ω due to the application of a unit normal concentrated load $\mathbf{p} = \delta(\mathbf{x}) \hat{\mathbf{e}}_3$ at the origin, including the effect of buoyancy at the surface. The boundary conditions at the surface $\partial\Omega$, recast in terms of stress components, is

$$\begin{aligned} \sigma_{13} &= 0, \\ \sigma_{23} &= 0, \\ \sigma_{33} &= -\delta(x_1)\delta(x_2) + \Delta\rho g u_3, \end{aligned} \quad (\text{A10})$$

where $\delta(x)$ is the Dirac delta function. We consider the case where the first two components of the Papkovitch potential vanish $B_1 = B_2 = 0$. The stress components become

$$\begin{aligned} \frac{\sigma_{13}}{\mu} &= (1 - \alpha) B_{3,1} - \alpha (x_3 B_{3,13} + B_{0,13}), \\ \frac{\sigma_{23}}{\mu} &= (1 - \alpha) B_{3,2} - \alpha (x_3 B_{3,23} + B_{0,23}), \\ \frac{\sigma_{33}}{\mu} &= B_{3,3} - \alpha (x_3 B_{3,33} + B_{0,33}). \end{aligned} \quad (\text{A11})$$

The displacement field is

$$\begin{aligned} u_1 &= -\frac{\alpha}{2} (x_3 B_{3,1} + B_{0,1}), \\ u_2 &= -\frac{\alpha}{2} (x_3 B_{3,2} + B_{0,2}), \\ u_3 &= \left(1 - \frac{\alpha}{2}\right) B_3 - \frac{\alpha}{2} (x_3 B_{3,3} + B_{0,3}). \end{aligned} \quad (\text{A12})$$

At the surface $x_3 = 0$, the stress components are simply

$$\begin{aligned} \frac{\sigma_{13}}{\mu} &= (1 - \alpha) B_{3,1} - \alpha B_{0,13}, \\ \frac{\sigma_{23}}{\mu} &= (1 - \alpha) B_{3,2} - \alpha B_{0,23}, \\ \frac{\sigma_{33}}{\mu} &= B_{3,3} - \alpha B_{0,33}, \end{aligned} \quad (\text{A13})$$

and the vertical displacement at the surface is

$$u_3 = \left(1 - \frac{\alpha}{2}\right) B_3 - \frac{\alpha}{2} B_{0,3}. \quad (\text{A14})$$

Note that the expressions $(1 - \alpha) B_{3,1} - \alpha B_{0,13}$ and $(1 - \alpha) B_{3,2} - \alpha B_{0,23}$ in eq. (A13) are harmonic in Ω and vanish at the surface $\partial\Omega$ due to the vanishing shear stress boundary condition (A10) on $\partial\Omega$. A harmonic field that vanishes at the domain boundary is zero identically in the whole domain and one obtains the relation

$$(1 - \alpha) B_3 - \alpha B_{0,3} = 0 \quad \text{in } \Omega. \quad (\text{A15})$$

Using Green’s third identity and the Betti’s method of integration (Love 1927, Chapter 10), the elastic response to load and gravity at the surface $\partial\Omega$ can be written

$$\frac{\sigma_{33}}{\mu} - 2\alpha\Gamma u_3 = \alpha (B_{3,3} - \Gamma B_3) = -\frac{1}{2\pi\mu} \frac{x_3}{r^3}, \quad (\text{A16})$$

where $r = (x_k x_k)^{1/2}$ is the distance from the point source (Fig. 1) and we have used the wavelength

$$\Gamma = \frac{\Delta\rho g}{2\mu\alpha}. \quad (\text{A17})$$

The component B_3 of the Papkovitch potential satisfies the inhomogeneous ordinary differential equation

$$B_{3,3} - \Gamma B_3 = -\frac{1}{2\pi\mu\alpha} \frac{x_3}{r^3}. \quad (\text{A18})$$

The homogeneous solution to eq. (A18) is associated with the trivial solution (zero displacements) of a stress-free boundary condition. Using the method of variation of parameters, the particular solution to (A18) is

$$B_3 = -\frac{e^{\Gamma x_3}}{2\pi\mu\alpha} \int_0^{x_3} \frac{t e^{-\Gamma t} dt}{(\rho^2 + t^2)^{3/2}}, \quad (\text{A19})$$

where

$$\rho = (x_1^2 + x_2^2)^{1/2}. \quad (\text{A20})$$

The definite integral in eq. (A19) does not readily yield a closed-form quadrature. An approximation of the solution to eq. (A18) is attainable by various ways. One is to Taylor-expand the denominator in the integrand in the right-hand-side of eq. (A19) and keep only the first two terms to obtain

$$B_3 \simeq -\frac{e^{\Gamma x_3}}{2\pi\mu\alpha} \int_0^{x_3} \frac{t e^{-\Gamma t} dt}{\rho(\rho^2 + \frac{3}{2}t^2)} \quad (\text{A21})$$

for which a solution can be expressed in closed form. However, for the sake of interpretation, we are looking for an expression

that can be separated into two parts, one part corresponding to the solution with no buoyancy effects ($\Gamma = 0$) and another part describing the contribution of gravity. Assuming that $\Gamma L \ll 1$, where L is the characteristic linear dimension of the problem, we use a perturbation approach (Bender & Orszag 1978) and write the successive approximations of B_3 as follows:

$$B_{3,3}^{(n+1)} = -\frac{1}{2\pi\mu\alpha} \frac{x_3}{r^3} + \Gamma B_3^{(n)} \quad (\text{A22})$$

with $B_3^{(0)} = 0$, where superscript $f^{(n)}$ denotes the approximation n of function f . The first approximation is

$$B_3^{(1)} = \frac{1}{2\pi\mu\alpha} \int_0^{x_3} \frac{-t dt}{(\rho^2 + t^2)^{3/2}} = \frac{1}{2\pi\mu\alpha} \frac{1}{r} \quad (\text{A23})$$

which corresponds to the well-known case where buoyancy at the surface is ignored (Love 1927; Mindlin 1936a; Nemat-Nasser & Hori 1999). The second approximation is

$$B_3^{(2)} = \frac{1}{2\pi\mu\alpha} \left[\int_0^{x_3} \frac{-t dt}{(\rho^2 + t^2)^{3/2}} + \Gamma \int_0^{x_3} \frac{dt}{(\rho^2 + x_3^2)^{1/2}} \right] \\ = \frac{1}{2\pi\mu\alpha} \left[\frac{1}{r} + \Gamma \ln(x_3 + r) \right] \quad (\text{A24})$$

and corresponds to our analytic approximation of the effect of gravity for the Boussinesq's problem; thereafter we use the approximation $B_3 \approx B_3^{(2)}$. Using eq. (A15) we define

$$B_0^{(n)} = \frac{1-\alpha}{\alpha} \int_0^{x_3} B_3^{(n)}(t) dt \quad (\text{A25})$$

to obtain

$$B_0^{(2)} = \frac{1-\alpha}{2\pi\mu\alpha^2} [\ln(x_3 + r) + \Gamma(x_3 \ln(x_3 + r) - r)]. \quad (\text{A26})$$

Finally, plugging eqs (A24) and (A26) into eq. (A12) and using the cylindrical coordinates we obtain the following approximation of the displacement field

$$u_r = \frac{\rho}{4\pi\mu r} \left[\frac{x_3}{r^2} - \frac{1-\alpha}{\alpha} \frac{1-\Gamma r}{x_3+r} - \Gamma \frac{x_3}{x_3+r} \right], \\ u_\theta = 0, \\ u_3 = \frac{1}{4\pi\mu r} \left[\alpha^{-1} + \frac{x_3^2}{r^2} + \Gamma [\alpha^{-1} r \ln(x_3 + r) - x_3] \right]. \quad (\text{A27})$$

For comparison, the Green's function of the Boussinesq's problem, in the absence of gravity, can be found, for example in Love (1927), Okumura (1995), Nemat-Nasser & Hori (1999) or Soutas-Little (1999)

$$u_r = \frac{\rho}{4\pi\mu r} \left[\frac{x_3}{r^2} - \frac{1-\alpha}{\alpha} \frac{1}{r+x_3} \right], \\ u_\theta = 0, \\ u_3 = \frac{1}{4\pi\mu r} \left[\alpha^{-1} + \frac{x_3^2}{r^2} \right]. \quad (\text{A28})$$

Note that eq. (A27) simplifies to the classic solution of eq. (A28) when $\Gamma = 0$, as expected.

A comparison between the Fourier-domain solution (eq. 29) and the corresponding analytic solution using the space-domain Green's function (eq. A27) is shown in Fig. A1. We compute the response of a point-source moment load \mathbf{m}_{13} applied at the surface $x_3 = 0$. We take into account a density contrast at the surface by setting $\Gamma = 10^{-2} \text{ m}^{-1}$. The corresponding displacement at a horizontal plane at a depth of 3 km is shown in Fig. A1(A). The difference between

the solution that includes a buoyancy effect and one that ignores buoyancy is shown in Fig. A1(B). The contribution of buoyancy to the total displacement field is less than 10 per cent of the total signal. The vertical displacement contribution of buoyancy is of opposite polarity compared with the direction of vertical displacement due to the direct effect of the applied traction. The buoyancy effect is tempering the amplitude of vertical displacement and the opposite polarity of the gravity contribution is an expected behaviour. We evaluate the contribution of gravity using our space-domain Green's function (A27). The residuals between the Fourier-domain and the space-domain solutions is shown in Fig. A1(C) and a comparison between the Fourier and space-domain solutions along profile C-C' is shown in Fig. A1(D). The residuals between the two fields are within a few percents of the maximum value of the gravity contribution field. Note a good agreement between the Fourier-domain and space domain solutions to the generalized Boussinesq's problem.

A3 From Fourier- to space-domain expressions

Finally, we establish the formal relation between the perturbation solution (A27) and the exact Fourier-domain solution (20), which we repeat here for convenience

$$\hat{u}_1(k_1, k_2, x_3) = i\alpha\omega_1\beta B_3 [1 - \alpha^{-1} + \beta x_3] e^{-\beta x_3}, \\ \hat{u}_2(k_1, k_2, x_3) = i\alpha\omega_2\beta B_3 [1 - \alpha^{-1} + \beta x_3] e^{-\beta x_3}, \\ \hat{u}_3(k_1, k_2, x_3) = -\alpha\beta^2 B_3 [\alpha^{-1} + \beta x_3] e^{-\beta x_3}. \quad (\text{A29})$$

Assuming small ratios of Γ/β , corresponding to a small wavelength limit, the constant

$$B_3 = \frac{-\hat{p}_3}{2\mu\alpha\beta^2(\beta + \Gamma)} \quad (\text{A30})$$

can be expanded in a Taylor series. Keeping the first two terms of the Taylor expansion we find

$$B_3 = \frac{-\hat{p}_3}{2\mu\alpha\beta^3} - \Gamma \frac{-\hat{p}_3}{2\mu\alpha\beta^4} + O\left(\frac{\Gamma^2}{\beta^2}\right). \quad (\text{A31})$$

Setting $p_3 = \delta(x_1)\delta(x_2)$, or simply $\hat{p}_3 = 1$, the first term corresponds to the classic Boussinesq's solution (A28) and the second term gives rise to the perturbation contribution found in eq. (A27). To illustrate this statement, we consider the vertical component of displacement. Using the expansion (A31) and setting $\hat{p}_3 = 1$, the vertical component of displacement in the Fourier domain becomes

$$\hat{u}_3(k_1, k_2, x_3) = \frac{1}{2\mu\beta} [\alpha^{-1} + \beta x_3] e^{-\beta x_3} \\ - \Gamma \frac{1}{2\mu\beta^2} [\alpha^{-1} + \beta x_3] e^{-\beta x_3}. \quad (\text{A32})$$

Upon inverse Fourier transforming with the pairs recalled in Table A1, we directly confirm that

$$u_3(x_1, x_2, x_3) = \frac{1}{4\pi\mu r} \left[\alpha^{-1} + \frac{x_3^2}{r^2} \right] \\ + \Gamma \frac{1}{4\pi\mu} \left[\alpha^{-1} \ln(x_3 + r) - \frac{x_3}{r} \right] \quad (\text{A33})$$

is the perturbation solution (eq. A27). Equivalence between the remaining components of displacement can be demonstrated in a similar way.

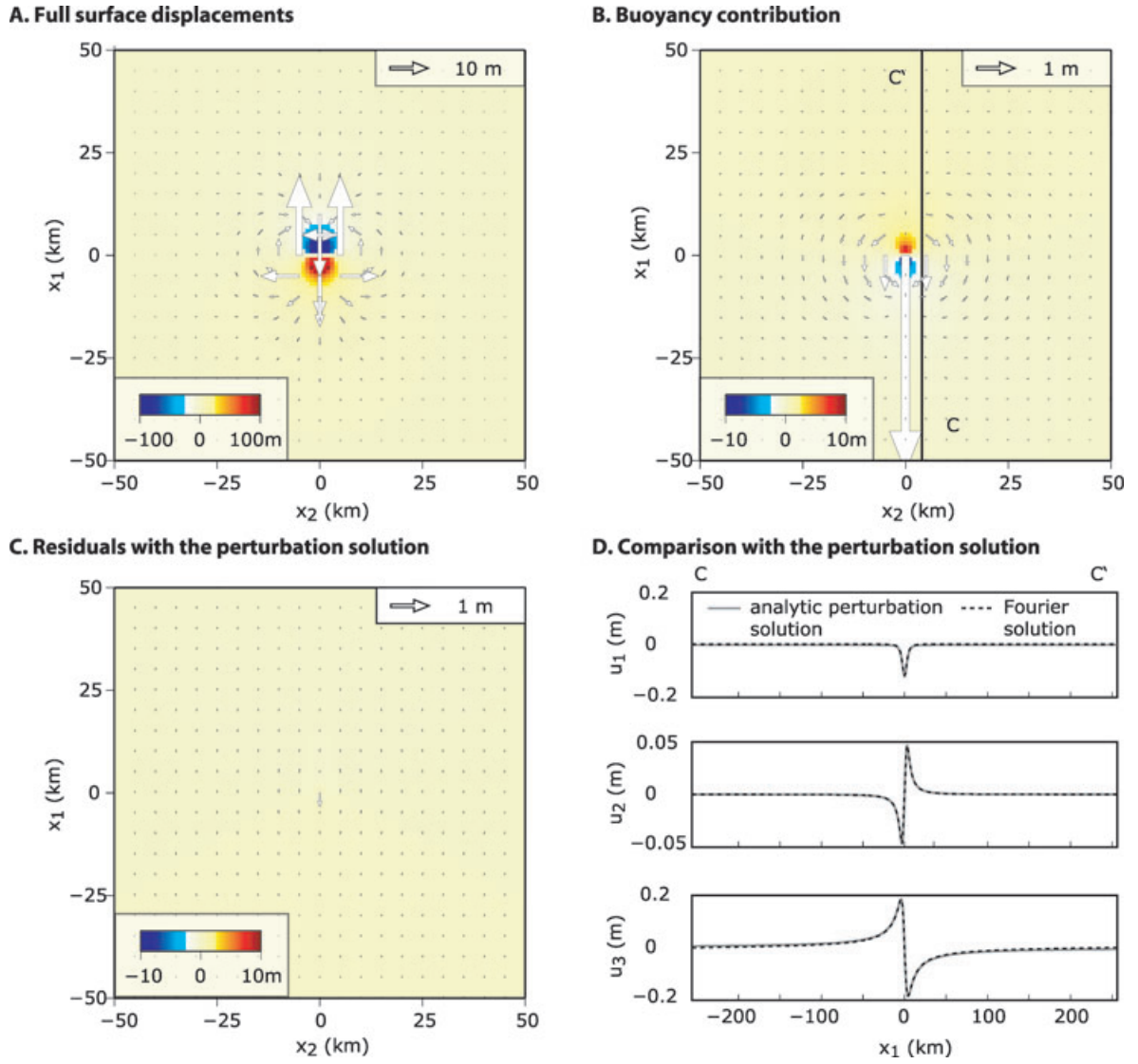


Figure A1. Benchmark of the Fourier-domain solution including a buoyancy boundary condition. (A) A moment \mathbf{m}_{13} is applied at the surface of the half-space. (B) The full surface displacement. Horizontal and vertical components of displacement are represented with arrows and colours, respectively (positive for uplift). (C) The surface displacement due to the surface buoyancy, corresponding to $\Gamma = 10^{-2} \text{ m}^{-1}$. Note the reversal of the vertical displacements. (D) The residuals between the Fourier-domain and the perturbation-method solutions, eqs (29) and (A27), respectively.

Table A1. Commonly used 2-D Fourier transforms of 3-D functions.

$f(x_1, x_2, x_3)$	$\mathcal{F}[f(\mathbf{x})] = \hat{f}(k_1, k_2, x_3)$
$1/r$	$\frac{1}{ \mathbf{k} } e^{-2\pi \mathbf{k} x_3}$
$\ln(x_3 + r)$	$\frac{1}{2\pi \mathbf{k} ^2} e^{-2\pi \mathbf{k} x_3}$
$x_3 \ln(x_3 + r) - r$	$\frac{1}{4\pi^2 \mathbf{k} ^3} e^{-2\pi \mathbf{k} x_3}$

Note: We denote $|\mathbf{k}| = (k_1^2 + k_2^2)^{1/2}$ and $r = (x_1^2 + x_2^2 + x_3^2)^{1/2}$. The Fourier transforms are defined in eq. (8).

APPENDIX B: STATIC DEFORMATION IN A HALF-SPACE DUE TO SURFACE TRACTION USING THE BOUSSINESQ–PAPKOVITCH–NEUBER POTENTIAL

In this appendix we use an alternative derivation of the Fourier domain solution for the Boussinesq’s and Cerruti’s problems. In Section 2, we used the Galerkin vector potential to derive the solution

to the generalized problem of applied surface traction including the effect of a buoyancy restoring force at the surface of a semi-infinite elastic solid. Here, we use the Boussinesq–Papkovitch–Neuber potential to derive the Fourier-domain solution to the Boussinesq’s and Cerruti’s problems, ignoring the effect of gravity. We use this alternative derivation to validate results of Section 2 in the special case where gravity is neglected (setting $\Gamma = 0$). We first derive the solution to the Boussinesq’s problem then to the Cerruti’s problem.

B1 The Boussinesq’s problem

The Boussinesq’s problem can be solved semi-analytically in the Fourier domain by making use of the Papkovitch–Neuber representation and Fourier transforming (A8) in the horizontal direction. Using the Fourier transforms pair defined in (8), the transformed gradient operator becomes $\hat{\nabla} = (i\omega_1, i\omega_2, \frac{\partial}{\partial x_3})$. In Cartesian coordinates, each component of the vector potential is harmonic and it is sufficient to set $\mathbf{B} = B_3 \mathbf{e}_3$. Hence, we have $\nabla^2 B_3 = \nabla^2 B_0 = 0$

and

$$\begin{aligned} \hat{B}_3(k_1, k_2, x_3) &= \beta b_3 e^{-\beta x_3}, \\ \hat{B}_0(k_1, k_2, x_3) &= b_0 e^{-\beta x_3}, \end{aligned} \tag{B1}$$

where we have used

$$\beta = 2\pi (k_1^2 + k_2^2)^{1/2}. \tag{B2}$$

We have discarded the positive exponentials to ensure a bounded solution in the far field. Before satisfying the surface boundary condition, we obtain the surface displacements

$$\begin{aligned} \hat{u}_1 &= -\alpha i\pi k_1 (b_0 + \beta b_3 x_3) e^{-\beta x_3}, \\ \hat{u}_2 &= -\alpha i\pi k_2 (b_0 + \beta b_3 x_3) e^{-\beta x_3}, \\ \hat{u}_3 &= +\beta \left[b_3 + \frac{\alpha}{2} (b_0 - b_3 + b_3 \beta x_3) \right] e^{-\beta x_3}. \end{aligned} \tag{B3}$$

At the surface, $x_3 = 0$, we have the shear stresses

$$\begin{aligned} \hat{\sigma}_{13} &= \mu i 2\pi k_1 \beta [\alpha b_0 + (1 - \alpha) b_3], \\ \hat{\sigma}_{23} &= \mu i 2\pi k_2 \beta [\alpha b_0 + (1 - \alpha) b_3], \end{aligned} \tag{B4}$$

so the condition of vanishing of the shear stress at the surface is satisfied for

$$b_0 = (1 - \alpha^{-1}) b_3. \tag{B5}$$

Respectively we obtain the displacement field

$$\begin{aligned} \hat{u}_1 &= -i\pi k_1 b_3 (\alpha - 1 + \alpha \beta x_3) e^{-\beta x_3}, \\ \hat{u}_2 &= -i\pi k_2 b_3 (\alpha - 1 + \alpha \beta x_3) e^{-\beta x_3}, \\ \hat{u}_3 &= +\frac{1}{2} \beta b_3 (1 + \alpha \beta x_3) e^{-\beta x_3}. \end{aligned} \tag{B6}$$

The surface normal stress, in the Fourier domain, is

$$\hat{\sigma}_{33} = -\mu \alpha \beta^2 b_3. \tag{B7}$$

Using the boundary condition $\sigma_{33}(x_1, x_2) = -p_3(x_1, x_2)$, where p_3 is the prescribed load at the surface, the Boussinesq problem is solved for

$$b_3 = \frac{\hat{p}_3}{\mu \alpha \beta^2}. \tag{B8}$$

Result (B6) is the same as the one of eq. (20) obtained using the Galerkin biharmonic vector potential.

B2 The Cerruti's problem

We start by considering the form of the solution corresponding to setting $B_2 = B_3 = 0$. The remaining non-zero harmonic scalar are thus

$$\begin{aligned} \hat{B}_0 &= b_0 e^{-\beta x_3}, \\ \hat{B}_1 &= \beta b_1 e^{-\beta x_3}, \end{aligned} \tag{B9}$$

making use of the Fourier transform identity

$$\mathcal{F}[2\pi x f(x)] = i \hat{f}'(k), \tag{B10}$$

where the prime means differentiation with respect to the relevant wavenumber, we obtain the displacements

$$\begin{aligned} \hat{u}_1 &= \left[\left(\beta + \frac{\alpha \omega_1^2}{2\beta} [1 - \beta x_3] \right) b_1 - \frac{\alpha}{2} i \omega_1 b_0 \right] e^{-\beta x_3}, \\ \hat{u}_2 &= -\frac{\alpha}{2} i \omega_2 \left[i \frac{\omega_1}{\beta} (1 - \beta x_3) b_1 + b_0 \right] e^{-\beta x_3}, \\ \hat{u}_3 &= -\frac{\alpha}{2} \left[i \omega_1 (-2 + \beta x_3) b_1 - \beta b_0 \right] e^{-\beta x_3}. \end{aligned} \tag{B11}$$

Using the Hooke's law for a homogeneous solid, we obtain the surface shear stresses

$$\begin{aligned} \hat{\sigma}_{13} &= \mu [i \omega_1 \alpha \beta b_0 - (\beta^2 + 2\omega_1^2 \alpha) b_1], \\ \hat{\sigma}_{23} &= \mu i \omega_1 \alpha (b_0 \beta + i 2\omega_1 b_1). \end{aligned} \tag{B12}$$

The vanishing condition for σ_{23} at the surface gives

$$b_0 = -\frac{i 2\omega_1}{\beta} b_1 \tag{B13}$$

and the prescribed surface stress $\hat{\sigma}_{13} = -\hat{p}_1$ gives

$$b_1 = \frac{\hat{p}_1}{\mu \beta^2}. \tag{B14}$$

The remaining normal stress is

$$\hat{\sigma}_{33} = -(1 - \alpha) i \omega_1 \beta b_1 = (\alpha - 1) \frac{i \omega_1 \hat{p}_1}{\mu \beta} \tag{B15}$$

and is removed by applying the Boussinesq's solution with the constant

$$b_3 = \frac{\alpha - 1}{\alpha} \frac{i \omega_1 \hat{p}_1}{\mu \beta^3}. \tag{B16}$$

The solution to Cerruti's problem, coming from the application of the Papkovitch–Neuber representation, is then

$$\begin{aligned} \hat{u}_1 &= \left[\frac{b_1}{\beta} \left(\beta^2 - \frac{\alpha}{2} \omega_1^2 (1 + \beta x_3) \right) - \frac{1}{2} i \omega_1 b_3 (\alpha - 1 + \alpha \beta x_3) \right] e^{-\beta x_3}, \\ \hat{u}_2 &= \left[-\frac{\alpha b_1}{2\beta} \omega_1 \omega_2 (1 + \beta x_3) - \frac{1}{2} i \omega_2 b_3 (\alpha - 1 + \alpha \beta x_3) \right] e^{-\beta x_3}, \\ \hat{u}_3 &= \frac{\alpha \beta}{2} \left[-i \omega_1 b_1 + b_3 (\alpha^{-1} + \beta x_3) \right] e^{-\beta x_3}. \end{aligned} \tag{B17}$$

Formulation (B17) is equivalent to eq. (26) obtained with the Galerkin vector potential. This alternative route to derive the homogeneous solution to the Navier's equation provides an independent check to validate our analytic solutions.